Accuracy assessment of different CBCT acquisition protocols used in rapid prototyping models

Avaliação da precisão de diferentes protocolos de aquisição de TCFC usados em modelos de prototipagem rápida

Evaluación de la precisión de diferentes protocolos de adquisición CBCT utilizados en modelos de creación rápida de prototipos

Paola Fernanda Leal Corazza

ORCID: https://orcid.org/0000-0002-8639-8392

São Leopoldo Mandic College, Brazil

E-mail: paola_corazza@hotmail.com

Fernando Martins Baeder

ORCID: https://orcid.org/0000-0001-7101-5689

Universidade Cruzeiro do Sul, Brasil

E-mail: fernandobaeder@uol.com.br

Daniel Furtado Silva

ORCID: https://orcid.org/0000-0003-3319-2996

Federal University of Paraíba, Brazil

E-mail: furtado.ds@gmail.com

Ana Carolina Lyra de Albuquerque

ORCID: https://orcid.org/0000-0002-6532-5020

Federal University of Campina Grande, Brazil

E-mail: lina.lyra@gmail.com

Jorge Vicente Lopes Silva

ORCID: https://orcid.org/0000-0002-2347-5215

Renato Archer Information Technology Center, Brazil

E-mail: jorge.silva@cti.gov.br

José Luiz Cintra Junqueira

ORCID: https://orcid.org/0000-0001-6788-4021

São Leopoldo Mandic College, Brazil

E-mail: joseluiz@slmandic.edu.br

Francine Kühl Panzarella

ORCID: https://orcid.org/0000-0002-5650-7711

São Leopoldo Mandic College, Brazil

E-mail: francine.panzarella@gmail.com

Abstract

This study compared the acquisition protocols of the Conical Beam Computed Tomography (CBCT) system, to assess the influence on image accuracy by different voxel sizes and the presence of soft tissue. Tomographic acquisition was performed in a fresh (F) and dry (D) pork jaw with voxel sizes of 0.4, 0.3 and 0.25 mm. The gold standard was obtained by scanning dry jaws covered with barium sulfate with a voxel size of 0.25 mm. The images were treated in the MIMICS® program, and noise areas were removed manually, using a fixed threshold for the purpose of generating 3D printing windows. Each window was virtually overlaid with the gold standard using the MeshLab software, obtaining absolute error values between the meshes, generating a map of discrepancies. Significant differences were found between windows D 0.30 vs. F 0.30, D 0.30 vs. F 0.25, D 0.30 vs. D 0.25, D 0.30 vs. F 0.40, F 0.30 vs. D 0.25, F 0.25 vs. D 0.25, F 0.25 vs. D 0.40, D 0.25 vs. F 0.40, D 0.25 vs. D 0.40 and F 0.40 vs. D 0.40, ($p < 0.05$). It was observed that the dry jaw windows showed a lower mean and standard deviation when compared to the fresh jaw windows. The 0.25 mm voxel protocol showed the most accurate result and the presence of soft tissues influenced the accuracy of the image when some protocols were compared statistically.

Keywords: Rapid prototyping; Cone beam computed tomograph; Voxel size; Soft tissue simulation.

Resumo

Este estudo comparou os protocolos de aquisição do sistema de Tomografia Computadorizada de Feixe Cônico (TCFC), para avaliar a influência na precisão da imagem por diferentes tamanhos de voxel e presença de tecido mole. A aquisição tomográfica foi realizada em mandíbula de porco nos estados fresco (F) e seco (D) com tamanhos de voxels de 0,4, 0,3 e 0,25 mm. O padrão ouro foi obtido pela varredura de mandíbula seca coberta com sulfato de bário com tamanho de voxel de 0,25 mm. As imagens foram tratadas no programa MIMICS®, e áreas de ruído foram removidas manualmente, utilizando limiar fixo para fins de geração de janelas de impressão 3D. Cada janela foi sobreposta virtualmente ao padrão ouro por meio do software MeshLab, obtendo-se valores de erros absolutos entre as malhas, gerando um mapa

de discrepâncias. Foram encontradas diferenças significativas entre as janelas D 0,30 vs. F 0,30, D 0,30 vs. F 0,25, D 0,30 vs. D 0,25, D 0,30 vs. F 0,40, F 0,30 vs. D 0,25, F 0,25 vs. D 0,25, F 0,25 vs. D 0,40, D 0,25 vs. F 0,40, D 0,25 vs. D 0,40 e F 0,40 vs. D 0,40, (p <0,05). Observou-se que as janelas de mandíbula seca apresentaram menor média e desvio padrão dos quando comparadas às janelas de mandíbula frescas. O protocolo com voxel de 0,25 mm apresentou o resultado mais acurado e a presença de tecidos moles influenciou na acurácia da imagem quando alguns protocolos foram comparados estatisticamente.

Palavras-chave: Prototipagem rápida; Tomógrafo computadorizado de feixe cônico; Tamanho do voxel; Simulação de tecido mole.

Resumen

Este estudio comparó los protocolos de adquisición del sistema de tomografía computarizada de haz cónico (TCHC), para evaluar la influencia en la precisión de la imagen por diferentes tamaños de voxel y la presencia de tejido blando. La adquisición tomográfica se realizó en mandíbula de cerdo fresca (F) y seca (D) con voxel de tamaños 0,4, 0,3 y 0,25 mm. El patrón oro se obtuvo escaneando mandíbulas secas cubiertas con sulfato de bario con tamaño de vóxel de 0,25 mm. Las imágenes se trataron en el programa MIMICS®, las áreas de ruido se eliminaron manualmente, utilizando un umbral fijo con el fin de generar ventanas de impresión 3D. Cada ventana se superpuso virtualmente con el estándar de oro utilizando software MeshLab, obteniendo valores absolutos de error entre las mallas, generando un mapa de discrepancias. Se encontraron diferencias significativas entre ventanas D 0,30 vs. F 0,30, D 0,30 vs. F 0,25, D 0,30 vs. D 0,25, D 0,30 vs. F 0,40, F 0,30 vs. D 0,25, F 0,25 vs. D 0,25, F 0,25 vs. D 0,40, D 0,25 vs. F 0,40, D 0,25 vs. D 0,40 y F 0,40 vs. D 0,40, (p <0,05). Se observó que las ventanas de mandíbula seca mostraron una desviación media y estándar más baja en comparación con ventanas de la mandíbula fresca. El protocolo de vóxel de 0,25 mm mostró el resultado más preciso y la presencia de tejidos blandos influyó en la precisión de la imagen cuando se compararon estadísticamente algunos protocolos.

Palabras clave: Creación rápida de prototipos; Tomógrafo computarizado de haz cónico; Tamaño de voxel; Simulación de tejidos blandos.

1. Introduction

Costs reduction is a crucial measure for attaining widespread use of medical applications of Rapid Prototyping (RP) in developing countries. The RP applications used in

medicine consist of building so-called biomodels, which are 3D physical models of the injured region of the body, such as those required in maxillofacial prosthetics and in the fabrication of implant surgical guides, so that the surgeon can plan and rehearse the surgery in advance (Chai et al., 2020; Morea et al., 2011; Skjerven, Riis, Herlofsson & Ellingsen,2019; Van der Meer et al., 2012; Weitz et al., 2011). This is a less invasive and less time-consuming surgical procedure, in addition to improving communications between patients and doctors (Zeng et al., 2012). High resolution three-dimensional (3D) images can further improve the ability to build biomodels. The construction of this type of model requires the integration of image acquisition with tomography equipment, software for medical image processing and rapid prototyping techniques.

A 3D image is composed of a stack of 2D images or slices, which were derived from DICOM files. In the same way that a 2D image is composed of pixels, a 3D image is composed of voxels. Each voxel has a gray-level value based on indirect calculation of the amount of radiation absorbed or captured by the charge couple device and calculated by means of a filtered-back projection algorithm. Visualization is based on a threshold filter. It is crucial to understand that the rendered image is the result of a user-entered threshold value. The operator's visual perception defines what is bone and what is soft tissue, and therefore, there are many factors that may affect this perception, such as the contrast of the image, noise in the image, individual visual perception and prior knowledge of anatomy among others (Ponce-Garcia et al., 2020; Taft, Kondor & Grant, 2011).

Recently, an impressive number of Cone Beam Computed Tomography (CBCT) scanners have been introduced in the field of dentomaxillofacial radiology and the important influence of voxel size on the quality of CBCT images and on scanning and reconstruction times has been acknowledged (Hassan, Aziz, Ralib & Saat, 2011; Kamburoğlu & Yüksel, 2011), but the accuracy of the RP coming from DICOM files needs to be clearly established.

In view of the above considerations, the aim of the present study was to compare the acquisition protocols of a CBCT system used to obtain rapid prototyping models, and evaluate whether the image acquisition protocols with different voxel sizes and the presence of soft tissue have an influence on the accuracy of the image.

2. Materials and Methods

The study plan was approved by the Ethical Committee of São Leopoldo Mandic Dental School, Campinas, Brazil. A fresh pig head was donated for use in this research, after

the animal was slaughtered for human consumption. It was taken to the Oral Radiology Department for tomographic image acquisition with the appliance i-CAT® Model No. 9140-0000-0000R, Serial No. ICU070931 (Imaging Sciences, Hatfield, PA, USA).

2.1 Image acquisition

The head was placed on a shield specifically for scanning objects, using wooden spatulas to adjust the mouth so that it would remain in a semi-open position. Scanning was performed in accordance with the daily calibration protocol of each item of equipment, at a room temperature of 20.0 ± 0.5ºC, and the following acquisition protocols: FoV of 20 cm, at acquisition of 40s (voxel size 0.4 mm); FoV of 13 cm, at acquisition of 20s (voxel size 0.3 mm); FoV of 13 cm, at acquisition of 40s (voxel size 0.25 mm). After scanning the head, primary reconstruction was performed with maximum resolution and cuts 1.0 mm thick, obtaining axial images. The scan volumes were exported in DICOM 3 format.

Afterwards the mandible was dissected, and then a paint brush was used to cover the entire surface of the dry mandible uniformly with a layer of barium sulphate (JB Química Indústria e Comércio LTDA, Suzano, São Paulo, Lot No 100201), diluted with water in the approximate proportion of 80% barium sulphate and 20% water (Figure 1).

Figure 1. Dry mandible covered with barium sulphate.
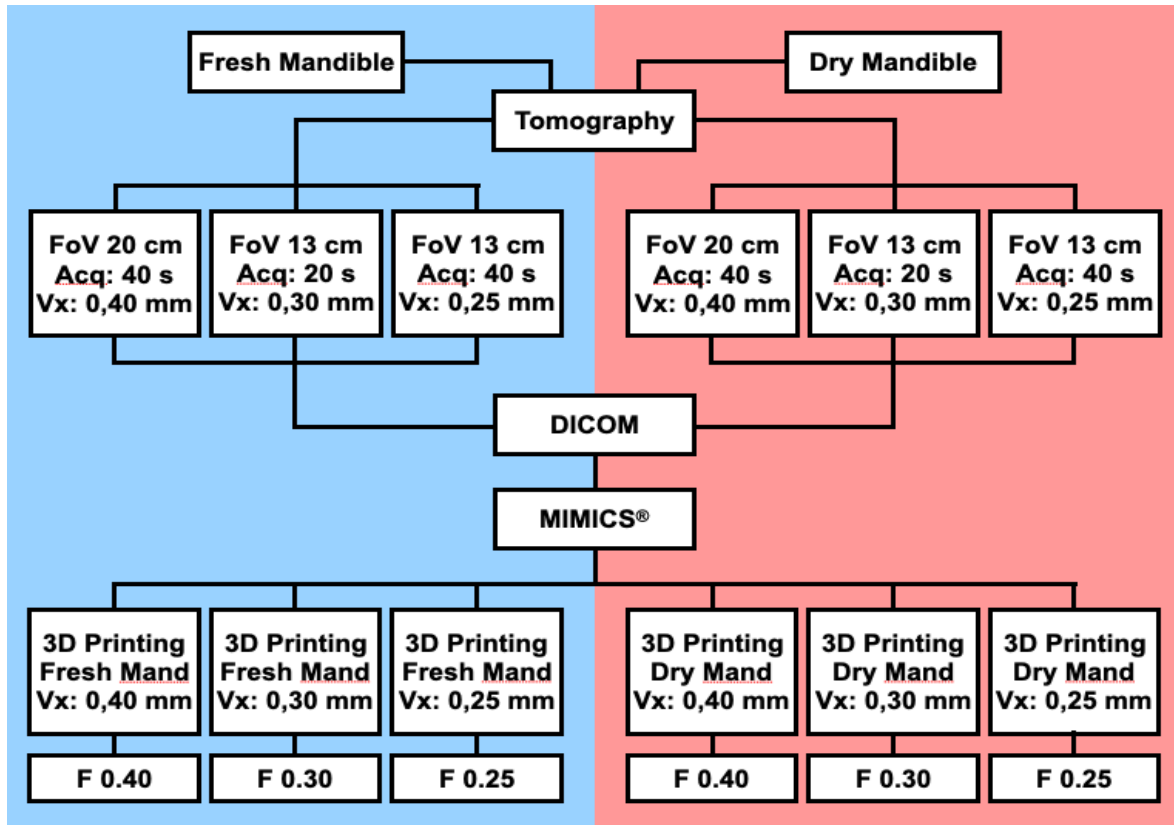

Source: Own authorship.

After covering the mandible with the contrast, the mandible was scanned again, using the protocol with a FoV of 13 cm, at acquisition of 40s (voxel size 0.25 mm) as this presents the smallest voxel size, a datum according to some studies (Hassan et al., 2010; Panzarella et al., 2011; Yi et al., 2017) which contributed to increasing the brightness.

Primary reconstruction was performed with maximum resolution, by means of cuts 1.0 mm thick, obtaining axial images of the entire acquisition. The scan volume was exported in DICOM 3 format.

2.2 Image processing and evaluation

The images of all the acquisitions were sent to the technology center (Centro de Tecnologia da Informação Renato Archer - CTI), which is a pioneer in Brazil in supporting public hospitals and developing applied research in medical applications of RP. These images were manipulated in the image treatment program MIMICS® (Materialise NV, Belgium), using an LCD SUN 19" Color Flat Panel Display monitor model L9ZF (Sun Microsystem Inc., Hillsboro, USA), with a 1280 x 1024 pixel resolution and a maximum color quality (32 bits). This image treatment, in which the areas of noise were removed, the procedure was manually performed by a single operator, using a fixed threshold for all the files, with the purpose of generating tridimensional geometries adequate for rapid prototyping; that is to say 3D Printing files (Diagram 1).

Diagram 1. Sequence for generating the 3D Printing files: Fresh Mandible with voxel size 0.4 mm (F 0.40); Fresh Mandible with voxel size 0.3 mm (F 0.30); Fresh Mandible with voxel size 0.25 mm (F 0.25); Dry Mandible with voxel size 0.4 mm (D 0.40); Dry Mandible with voxel size 0.3 mm (D 0.30); Dry Mandible with voxel size 0.25 mm (D 0.25).

Legend: -Acq: Acquisition; -Vx: Voxel; - Mand: Mandible. Source: Own authorship.

To compare the images obtained, the final analysis was performed using the free open source software called MeshLab® (Visual Computing Lab, ISTI, Pisa, Italy). This software is a platform for processing and editing unstructured 3D triangular meshes, as is the case of the geometries discussed in this article. To evaluate the precision of reproduction of the mandible, the data were compared using a discrepancy map (Figure 2).

Figure 2. Visualization of the discrepancy map.
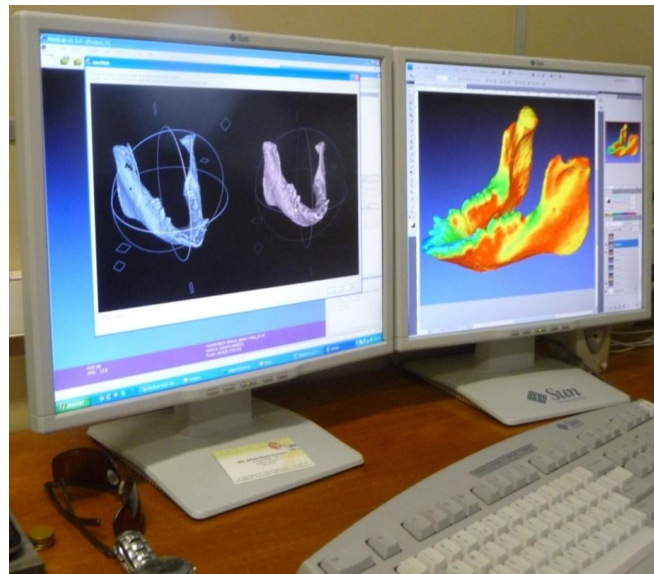
Source: Own authorship.

Using the analysis resources of the MeshLab® software, such as filters and visualization resources, the discrepancy map was obtained by virtually superimposing each of the 3D Printing files on the target (dry mandible with barium), thus obtaining absolute error values between one mesh and the other (Diagram 2).

Diagram 2. Comparison of protocols in relation to the gold standard.
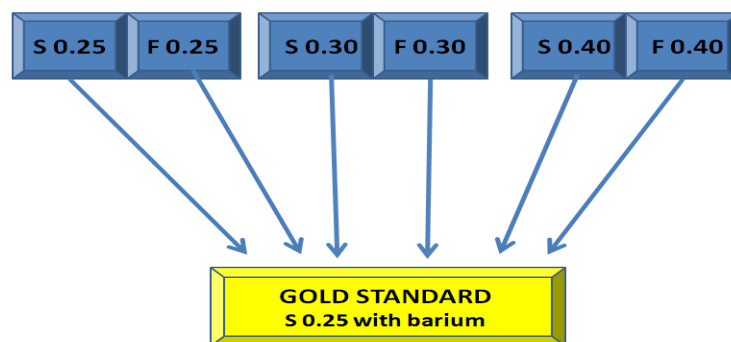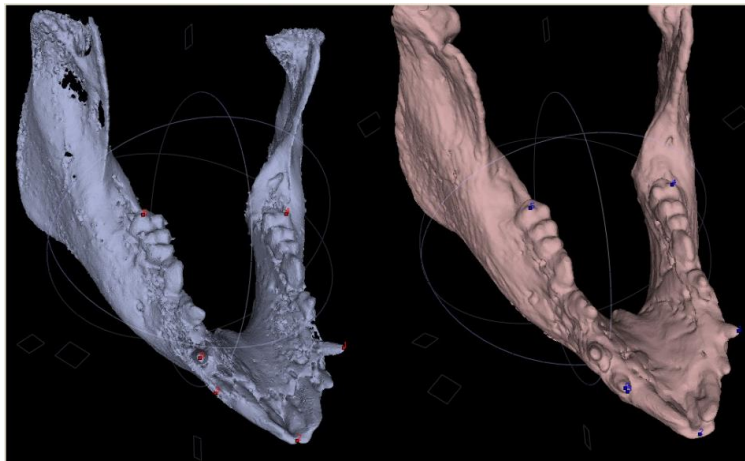

Source: Own authorship.

To compare the distances between the meshes; between the geometries obtained after noise removal by the MIMICS® program, the *Hausdorff Distance* Filter, a MeshLab® tool was used. This computer environment provides data such as: *Mesh Bounding Box Size*, *Mesh Bounding Box Diag*, *Mesh Volume* and *Mesh Surface*. All of these data are obtained in

millimeters, enabling collision (superimposition) of the images, and thus, generate the discrepancy map. After this the filter Colorize by Vertex Quality was used, which is a resource that colors the geometries by attributing the values obtained by the *Hausdorff Distance* Filter, to the mesh vertices.

The sum of the two filters produce images generated in the discrepancy map. For better visualization, in addition to the numerical information, the maps with the colors were used. To standardize the coloring process, the values used were from 0 to 3, according to the proximity between the mesh to be compared and the gold standard, being: 0 for the color red (corresponding to the area in which the meshes completely coincided), followed by 1 yellow, 2 green and 3 blue (the region of greatest distance between the meshes).
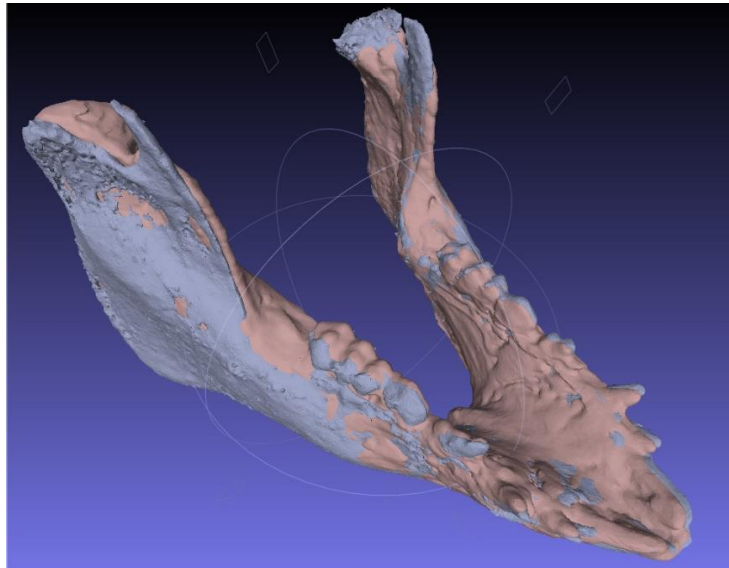
In the process of aligning the meshes and constructing the discrepancy map, 5 points of reference (Figure 3) were manually selected, to help the program with superimposing the images (Figure 4).

Figure 3. Selection of points of reference.

Source: Own authorship.

Figure 4. Superimposition of meshes.

Source: Own authorship.

2.3 Statistical analysis

The data relative to the measurements made in the tomographic images were submitted to descriptive statistical analysis. To compare the discrepancy maps of the dry and fresh mandible with the gold standard, the analysis of variance (ANOVA) was performed, and the level of significance was set at $p < 0.0001$. In addition, the Tukey-Kramer multiple comparisons test was performed. Differences were considered to be statistically significant when ($p < 0.05$).

3. Results

By means of analyzing the discrepancy maps generated by comparing the 3D Printing files with the gold standard, it was observed that the dry mandible files (D 0.25, D 0.30 and D 0.40) presented a lower mean and standard deviation of the points generated by the *Hausdorff Distance* filter, when compared with the fresh mandible files (F 0.25, F 0.30 and F 0.40) (Table 1).

Table 1. Mean ± standard deviations in millimeters of the *Hausdorff Distance* filter for analysis of the discrepancy maps of the 3D Printing files.

Protocols	Number of points	Mean	SD
D 0.25	287,246	0.20	0.31
D 0.30	65,531	0.33	0.37
D 0.40	123,954	0.43	0.45
F 0.25	372,817	0.54	0.64
F 0.30	65,532	0.49	0.52
F 0.40	143,177	0.54	0.54

3D Printing files: Fresh Mandible with voxel size 0.4 mm (F 0.40); Fresh Mandible with voxel size 0.3 mm (F 0.30); Fresh Mandible with voxel size 0.25 mm (F 0.25); Dry Mandible with voxel size 0.4 mm (D 0.40); Dry Mandible with voxel size 0.3 mm (D 0.30); Dry Mandible with voxel size 0.25 mm (D 0.25). Source: Own authorship.

To compare the discrepancy maps of the files with the gold standard in millimeters, the analysis of variance (ANOVA) test was applied. The variation between the means of the columns was significantly greater than had been expected and a significant difference ($p < 0.0001$) was found.

The Tukey-Kramer multiple comparisons test was applied and significant differences were found between files D 0.30 vs. F 0.30, D 0.30 vs. F 0.25, D 0.30 vs. D 0.25, D 0.30 vs. F 0.40, F 0.30 vs. D 0.25, F 0.25 vs. D 0.25, F 0.25 vs. D 0.40, D 0.25 vs. F 0.40, D 0.25 vs. D 0.40 e F 0.40 vs. D 0.40, ($p < 0.05$). Whereas, the protocols of D 0.30 vs. D 0.40, F 0.30 vs. F 0.25, F 0.30 vs. F 0.40, F 0.30 vs. D 0.40 and F 0.25 vs. F 0.40 showed no significant differences ($p > 0.05$) between them (Table 2).

**Table 2.** Comparison between the differences, in millimeters, generated by the discrepancy maps.

Comparison	Mean Difference	P value
D 0.30 vs. F 0.30	-0.1631	P<0.05
D 0.30 vs. F 0.25	-0.2098	P<0.001
D 0.30 vs. D 0.25	0.1307	P<0.05
D 0.30 vs. F 0.40	-0.2203	P<0.001
D 0.30 vs. D 0.40	-0.09837	P>0.05
F 0.30 vs. F 0.25	-0.04674	P>0.05
F 0.30 vs. D 0.25	0.2938	P<0.001
F 0.30 vs. F 0.40	-0.05719	P>0.05
F 0.30 vs. D 0.40	0.06470	P>0.05
F 0.25 vs. D 0.25	0.3405	P<0.001
F 0.25 vs. F 0.40	-0.01045	P>0.05
F 0.25 vs. D 0.40	0.1114	P<0.001
D 0.25 vs. F 0.40	-0.3509	P<0.001
D 0.25 vs. D 0.40	-0.2291	P<0.001
F 0.40 vs. D 0.40	0.1219	P<0.001

Source: Own authorship.

Considering that the smallest difference in millimeters compared with the gold standards represents the best method for obtaining the image, protocol D 0.25 presented the most accurate result when compared with the other methods, bearing in mind that it was statistically significant ($p < 0.05$) when compared with the other image acquisition techniques.
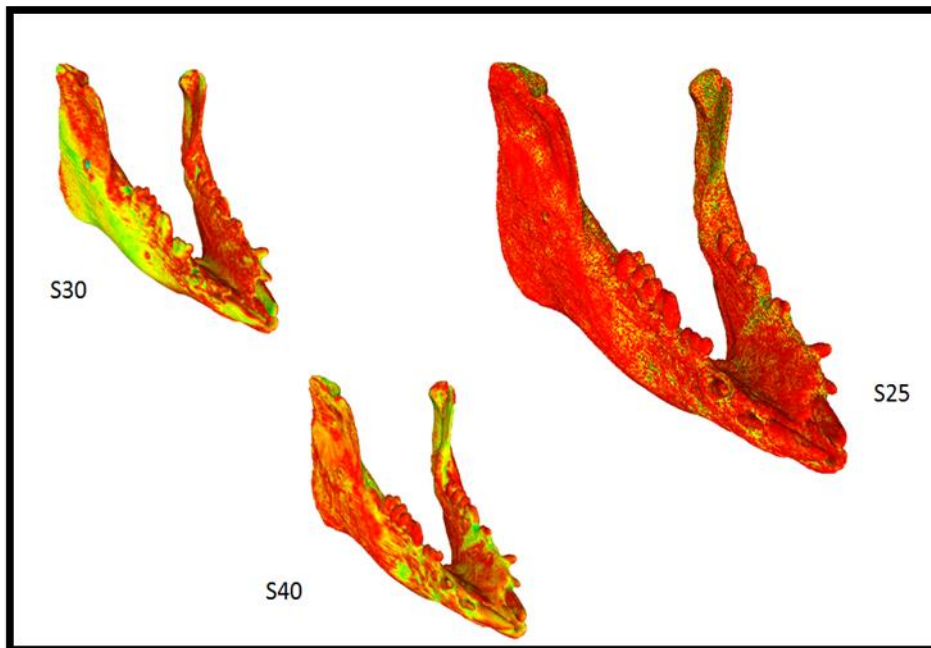
A color gradient was used to define and compare the accuracy of segmentation, with red representing the regions that coincided, and blue for the more distant regions, according to Figures 5 and 6.

Figure 5. Discrepancy maps between the fresh CT and gold standard.
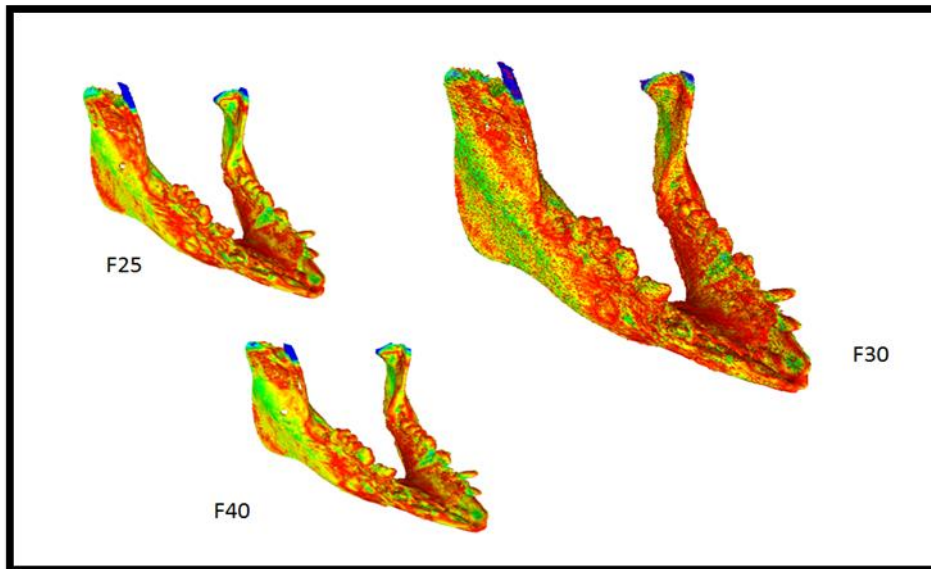
Source: Own authorship.

Figure 6. Discrepancy maps between the dry CT and gold standard.

Source: Own authorship.

4. Discussion

Based on results obtained, it was observed that the protocols of the dry mandible (D25, D30 and D40) presented a lower mean and standard deviation between the samples, of the points generated by the *Hausdorff Distance* filter, according to Table 1.

The difference in millimeters between the discrepancy maps was compared, according to Table 1, highlighting protocols F 0.30 and D 0.25 since they presented a smaller difference in millimeters compared with the gold standard, in comparison with the other fresh and dry protocols, respectively. The fresh mandible protocols (F 0.25 and F 0.40) were those that presented the regions that presented most discrepancy in comparison with the gold standard, suggesting there was influence of the soft tissue in these protocols, corroborating the results of the research of De Souza et al. (2004).

In the results presented in Table 1, it was observed that there was no relationship between the number of points and the difference in millimeters in the discrepancy map. Thus, one cannot affirm how much more precise the protocol was, how many more points there were in its mesh, or the lower the number of points was, the more distant the mesh would be from the gold standard.

For comparison of the 3D geometries with the gold standard, discrepancy maps were used, which enabled the regions of coincidence between the meshes to be visualized (*Colorize by Vertex Quality*) and their numerical quantification (*Hausdorff Distance),* based on the methodologies used by Liang et al. (2010). The results demonstrated in Figures 5 and 6 showed the discrepancy maps with more red areas, which corresponded to the regions with greater accuracy, and small colored areas, with blue presenting the area with least accuracy.

FoVs of 13 cm and 20 cm were used to compare different voxel sizes. The mandible was positioned in the center of the FoV to avoid the artifact truncated view issue (Loubele et al.,2008) and also ensure a higher spatial accuracy (Juerchott et al., 2018).

To achieve better brightness in obtaining the gold standard, a protocol with a smaller voxel size was chosen, since it contributed to increasing the brightness of the image, according to previous studies (Dawood, Patel & Brown, 2009; Hatcher, 2010; Maret et al., 2012; Panzarella et al., 2011; Watanabe, Honda & Kurabayashi, 2010). However, the study of Damstra, Fourie, Slater & Ren (2010) demonstrated that there was exactness between the measurements of the different voxels, irrespective of the resolution. Moreover, Hassan, Souza, Jacobs, Bert & Van der Stelt (2010) reported that anisotropic voxels with a small pixel

area in the *x,y* plane and larger slice thickness can be used instead of the "standard" small isotropic voxels, in order to maintain the image quality and reduce image noise.

The presence of significant differences was observed between D 0.30 vs. F 0.30; D 0.30 vs. F 0.25; D 0.30 vs. D 0.25; D 0.30 vs. F 0.40; F 0.30 vs. D 0.25; F 0.25 vs. D 0.25; F 0.25 vs. D 0.40; D 0.25 vs. F 0.40; D 0.25 vs. D 0.40 and F 0.40 vs. D 0.40 ($p<0.05$), according to Table 2. Considering that the smaller the difference in millimeters in comparison with the gold standard, the better is the method for obtaining the image, it was concluded that D 0.25 presented the best result when compared with the other methods, bearing in mind that it was statistically significant ($p<0.05$).

In the present study a single mandible was used in two different conditions: fresh and dry. This led to the comparison being most adequate, and also had the advantage of establishing pure comparisons. The use of fresh material allowed adequate parameters of reproducibility of some physical phenomena, such as attenuation of the X-ray beam, dispersed radiation and noise. Although some studies (De Souza et al., 2004; Ponce-Garcia et al., 2020) have also used soft tissue simulators in their experiments, one notes the absence of publications evaluating the interference of soft tissues in the quality and precision of images.

During image treatment, in which the areas of noise were removed, the procedure was manually performed by a single operator, using a fixed threshold for all the files, with the purpose of generating 3D Printing files used for fabricating rapid prototyping models.

The histogram of a CBCT dataset is composed of a wide range of gray-scale values that represent the X-ray attenuation profiles of the different soft and hard tissues. The equipment used in this research has 14 bits (2^{14} = 16,384 different gray tones) in which the real number of significant densities is limited by imprecision in image acquisition, and it is generally more difficult to specify the correct threshold value to separate the bone from soft tissue and background in CBCT than in conventional CT due to inherent inconsistencies in the histogram. Studies described in the literature (Damstra et al., 2010; Pitale et al., 2020), in which surface models were processed by a volumetric renderization program related that the smallest detectable difference in the CBCT measurements were minimal, confirming the exactness of the CBCT measuring process. Barbero & Ureta (2011), and Alsharbaty et al. (2019) affirmed that the dimensional error of CT mainly occurs due to the selection of minimum gray scale parameters that separate the noise right from the beginning of the contours of the part, and the easiest segmentation algorithm to use is the use of a global threshold value. This means that a single threshold value is used for the segment of the entire object in the entire image. According Bibb & Winder (2010) when using the threshold in the

processes of adjusting the image, removing noise and separating the different tissues, this may result in an alteration in the image in 3D reconstructions.

To understand the results, a supposition was formulated: the main reason for the limitation of CBCT with respect to the lower quality of reproduction of tissues is related to the formation of the digital image on the sensor. When the beam of rays passes through the object and attains the digital sensor of the equipment, electrical impulses are originated in order to produce the image on the computer. In the conversion of these impulses into an image, the binary digit of the CBCT is variable, and with inferior contrast resolution to that of medical CT. Therefore, the capacity to distinguish different densities in radiographic images will depend directly on the function of interaction of the characteristics of the coefficient of linear attenuation of the tissues that are being radiographed. It will also depend on the capacity of the image receptor to distinguish differences in numbers of photons of X-rays that come from different areas of the object, capacity of the monitor or other output device to depict these differences. In addition, it will depend on the human visual system, which is only capable of distinguishing approximately 60 levels of gray tones under ideal conditions, in order to perform an image treatment for the construction of the 3D mesh. A datum that corroborates the statement of Bibb & Winder (2010) when they affirmed that errors may occur due to the fact that the software is manipulated by a human being.

Generally, all methodologies have advantages and disadvantages, however previous studies (Ahmed & Ali, 2019; Barbero & Ureta, 2011; Bombeccari, Candotto, Giannì, Carinci & Spadari 2019; Brüllmann & Schulze, 2015; Damstra et al., 2010; Liang et al., 2010; Panzarella et al., 2011) presented results that might be applied to the clinic.

Although several manufacturers of scanning systems report on the effectiveness of their tools under optimal conditions, it is important to review the Barbero & Ureta (2011) since experiments with simple or complex objects of different materials produce results that might question the accuracy of these systems. The authors suggest future research CT to determine the minimum grayscale for each material and density, so that CT can be used as a tool for reverse engineering more accurately.

There are few studies based on dry skull samples that have assessed the accuracy of 3D model reconstructions from CBCT (Doyle, Wiltz & Kraut, 2015; García-Sanz et al., 2017). It is difficult to make a comparative analysis of the data described in the literature with the present study due to the great difference in the experimental designs cited for evaluating the precision of tomographic images. Indeed, this should be one of the concerns of researchers in the area: establish a standardized methodology that allows comparison of studies, and

consequently, great advancement in scientific researches.

5. Conclusion

In conclusion, the protocol with voxel size 0.25 mm presented the most accurate result and presence of soft tissue influenced the image accuracy in some protocols.

References

Ahmed, M., & Ali, S. (2019). Computer guided temporomandibular joint reconstruction of Kaban III hemifacial microsomia with anotia: A case report. *Int J Surg Case Rep*, 57, 52-56.

Alsharbaty, M. H. M., Alikhasi, M., Zarrati, S., & Shamshiri, A. R. (2019). A clinical comparative study of 3-dimensional accuracy between digital and conventional implant impression techniques. *J Prosthodont*, 28(4), e902-e908.

Barbero, B. R., Ureta, E. S. (2011). Comparative study of different digitization techniques and their accuracy. *Computer-Aided Desing*, 43(2), 188-206.

Bibb, R., Winder, J. (2010). A review of the issues surrounding three-dimensional computed tomography for medical modelling using rapid prototyping techniques. *Radiography*, 16(1), 78-83.

Bombeccari, G. P., Candotto, V., Giannì, A. B., Carinci, F., & Spadari, F. (2019). Accuracy of the cone beam computed tomography in the detection of bone invasion in patients with oral cancer: a systematic review. *Eurasian J Med*, 51(3), 298-306.

Brüllmann, D., & Schulze, R. K. (2015). Spatial resolution in CBCT machines for dental/maxillofacial applications-what do we know today? *Dentomaxillofac Radiol*, 44(1), 20140204.

Chai, J., Liu, X., Schweyen, R., Setz, J., Pan, S., Liu, J., & Zhou, Y. (2020). Accuracy of implant surgical guides fabricated using computer numerical control milling for edentulous jaws: a pilot clinical trial. *BMC oral health*, 20(1), 288.

Damstra, J., Fourie, Z., Slater, J. J. R. H., & Ren, Y. (2010). Accuracy of linear measurements from cone-beam computed tomography-derived surface models of different voxel sizes. *Am J Orthod Dentofacial Orthop*, 137(1), 16.e1-16.e6.

Dawood, A., Patel, S., & Brown, J. (2009). Cone beam CT in dental practice. *Br Dent J*, 207(1), 23-8. doi: 10.1038/sj.bdj.2009.560. PMID: 19590551.

De Souza, L. R. M. F., Faintuch, S., Nicola, H., Bekhor, D., Tiferes, D. A., Goldman, S. M., Ajzen, A. S., & Szejnfeld, J. (2004). A tomografia computadorizada helicoidal no diagnóstico da litíase ureteral. *Rev Imagem*, 26(4), 315-321.

Doyle, S., Wiltz, M. J. & Kraut, R. A. (2015). Comparison of cone-beam computed tomography and multi-slice spiral computed tomography bone density measurements in the maxilla and mandible. *N Y State Dent J*, 81(4), 42-5.

Fernandes, T. M., Adamczyk, J., Poleti, M. L., Henriques, J. F., Friedland, B., & Garib, D. G. (2015). Comparison between 3D volumetric rendering and multiplanar slices on the reliability of linear measurements on CBCT images: an in vitro study. *J Appl Oral Sci*, 23(1), 56-63.

García-Sanz, V., Bellot-Arcís, C., Hernández, V., Serrano-Sánchez, P., Guarinos, J., & Paredes-Gallardo, V. (2017). Accuracy and Reliability of Cone-Beam Computed Tomography for Linear and Volumetric Mandibular Condyle Measurements. A Human Cadaver Study. *Scientific reports*, 7(1), 11993.

Hassan, B., Souza, C. P., Jacobs, R., Berti, S. A., & Van der Stelt, P. (2010). Influence of scanning and reconstruction parameters on quality of three-dimensional surface models of the dental arches from cone beam computed tomography. *Clin Oral Investig*, 14(3), 303-10.

Hassan, R., Aziz, A. A., Ralib, A. R. M., & Saat, A. (2011). Computed tomography of blunt spleen injury: a pictorial review. *Malay J Med Sci*, 18(1), 60–67.

Hatcher, D C. (2010). Operational principles for cone-beam computed tomography. *J Am Dent Assoc*, 141(Suppl 3), 3S-6S.

Juerchott, A., Saleem, M. A., Hilgenfeld, T., Freudlsperger, C., Zingler, S., Lux, C. J., Bendszus, M., & Heiland, S. (2018). 3D cephalometric analysis using Magnetic Resonance Imaging: validation of accuracy and reproducibility. *Sci Rep*, 8(1), 13029.

Kamburoğlu, K., & Yüksel, S. (2011). A comparative study of the accuracy and reliability of multidetector CT and cone beam CT in the assessment of dental implant site dimensions. *Dentomaxillofac Radiol*, 40(7), 466–9.

Loubele, M., Asseche, N. V., Carpentier, K., Maes, F., Jacobs, R., Steenberghe, D. V., & Suetens, P. (2008). Comparative localized linear accuracy of small-field cone-beam CT and multislice CT for alveolar bone measurements. *Oral Surg Oral Med Oral Pathol Oral Radiol Endod*, 105(4), 512-8.

Liang, X., Lambrichts, I., Sun, Y., Denis, K., Hassan, B., Li, L., Pauwels, R., & Jacobs, R. (2010). A comparative evaluation of Cone Beam Computed Tomography (CBCT) and Multi-Slice CT (MSCT). Part II: On 3D model accuracy. *Eur J Radiol*, 75(2), 270-4.

Maret, D., Telmon, N., Peters, O. A., Lepage, B., Treil, J., Inglèse, J. M., Peyre, A., Kahn, J. L., & Sixou, M. (2012). Effect of voxel size on the accuracy of 3D reconstructions with cone beam CT. *Dentomaxillofac Radiol*, 41(8), 649-55.

Morea, C., Hayek, J. E., Oleskovicz, C., Dominguez, G. C., & Chilvarquer, I. (2011). Precise insertion of orthodontic miniscrews with a stereolithographic surgical guide based on cone beam computed tomography data: a pilot study. *Int J Oral Maxillofac Implants*, 26(4), 860-5.

Panzarella, F. K., Junqueira, J. L. C., Oliveira, L. B., Araujo, N. S., & Costa, C. (2011). Accuracy assessment of the axial images obtained from cone beam computed tomography. *Dentomaxillofac Radiol*, 40(6), 369-78.

Pitale, U., Mankad, H., Pandey, R., Pal, P. C., Dhakad, S., & Mittal, A. (2020). Comparative evaluation of the precision of cone-beam computed tomography and surgical intervention in the determination of periodontal bone defects: A clinicoradiographic study. *Journal of Indian Society of Periodontology*, 24(2), 127–34.

Ponce-Garcia, C., Ruellas, A., Cevidanes, L., Flores-Mir, C., Carey, J. P., & Lagravere-Vich, M. (2020). Measurement error and reliability of three available 3D superimposition methods in growing patients. *Head & face medicine*, 16(1), 1

Skjerven, H., Riis, U. H., Herlofsson, B. B., & Ellingsen, J. E. (2019). In vivo accuracy of implant placement using a full digital planning modality and stereolithographic guides. *Int J Oral Maxillofac Implants*, 34(1), 124-32.

Taft, R. M., Kondor, S. & Grant, G. T. (2011). Accuracy of rapid prototype models for head and neck reconstruction. *J Prosthet Dent*, 106 (6), 399-408.

Van der Meer, W. J., Vissink, A., Raghoebar, G. M., & Visser, A. (2012). Digitally designed surgical guides for placing extraoral implants in the mastoid area. *Int J Oral Maxillofac Implants*, 27(3), 703-7.

Watanabe, H., Honda, E., & Kurabayashi, T. (2010). Modulation transfer function evaluation of cone beam computed tomography for dental use with the oversampling method. *Dentomaxillofac Radiol*, 39(1), 28-32.

Weitz, J., Deppe, H., Stopp, S., Lueth, T., Mueller, S., & Hohlweg-Majert, B. (2011). Accuracy of templates for navigated implantation made by rapid prototyping with DICOM datasets of cone beam computer tomography (CBCT). *Clin Oral Investig*, 15(6), 1001-6.

Yi, J., Sun, Y., Li, Y., Li, C., Li, X., & Zhao, Z. (2017). Cone-beam computed tomography versus periapical radiograph for diagnosing external root resorption: A systematic review and meta-analysis. *Angle Orthod*, 87(2), 328-37.

Zeng, F. H., Xu, Y. Z., Fang, L., & Tang, X. S. (2012). Reliability of three dimensional resin model by rapid prototyping manufacturing and digital modeling. *Shanghai Kou Qiang Yi Xue*, 21(1), 53-6.

Percentage of contribution of each author in the manuscript

Paola Fernanda Leal Corazza – 18%

Fernando Martins Baeder – 18%

Daniel Furtado Silva – 5%

Ana Carolina Lyra de Albuquerque – 5%

Jorge Vicente Lopes Silva – 18%

José Luiz Cintra Junqueira – 18%

Francine Kühl Panzarella – 18%